

Reverse conducting lateral insulated-gate bipolar transistors with a non-local band-to-band tunnelling junction

Qiang Fu, Bo Zhang, Ming Qiao, Xuan Li, Xiaorong Luo, Zhaoji Li

State Key Laboratory of Electronic Thin Films and Integrated Devices, University of Electronic Science and Technology of China, Chengdu 610054, People's Republic of China
E-mail: fuqiang17@gmail.com

Published in Micro & Nano Letters; Received on 2nd March 2014; Revised on 20th June 2014; Accepted on 21st July 2014

A new reverse conducting lateral insulated-gate bipolar transistor (LIGBT) structure with a non-local band-to-band tunnelling junction is proposed and its operating principle is demonstrated in detail for a power-switching device. By utilising the reverse bias characteristics of the tunnelling junction, the proposed LIGBT can operate successfully in the freewheeling diode mode without an external anti-parallel diode. Analysis has illustrated that the proposed LIGBT can achieve a reverse knee voltage of -1 V and a lower reverse conduction voltage drop of -1.4 V at a current density of 100 A/cm^2 . It also shows a good temperature effect on the forward and reverse current. Moreover, it exhibits a better soft reverse recovery performance and about two times higher soft factor than the lateral P-i-N diode.

1. Introduction: Lateral insulated-gate bipolar transistors (LIGBTs) on silicon-on-insulator (SOI) have been widely used in integrated power integrated circuits (ICs) because of their ease of integration, high current handling capability, high reliability and superior isolation [1, 2]. In mid-high voltage power applications (ranging from 200 to 900 V), they are typically implemented in the output stages of driver ICs for inverters, pulse-width modulation converters and motor controls [3–5]. However, from a system application standpoint it is necessary to integrate the anti-parallel diode across the insulated-gate bipolar transistor (IGBT) structure to carry the load current during a part of the operating cycle and eliminate an additional component in the system. When compared with metal oxide semiconductor field effect transistors, they do have to connect an anti-parallel diode across the IGBT structure and this leads to additional area consumption to accommodate the on-chip diodes. Consequently, lots of reverse conducting vertical IGBTs and the shorted anode LIGBTs have been proposed and discussed [6–8]. However, it is difficult to keep the snap-back voltage very low and optimise the same silicon for both the modes while maintaining good reverse conduction through the body diode. Besides, because of the frequent switching of devices the current convergence effect in the shorted anode region may be another major problem.

The quantum band-to-band tunnelling (BTBT) phenomenon, which was first observed more than 50 years ago in the p–n junction diode by Esaki [9], operates by having electrons travel through the forbidden bandgap. Recently, a number of research efforts have been made to integrate the quantum tunnelling effects into complementary metal oxide semiconductor devices (e.g. tunnel field-effect transistors) [10–13]. However, the reverse-biased tunnelling has received much less attention until recently and only a few efforts were made for power semiconductor devices [14–16].

In this Letter, we propose a particular LIGBT (named the tunnel-LIGBT) that utilises a reverse-biased quantum BTBT effect in the p–n junction to make the LIGBT have the reverse conducting and reverse recovery performances.

2. Device structure and operating principle: The schematic cross-section of the tunnel-LIGBT on SOI is shown in Fig. 1. The x -, y - and z -directions are also given in Fig. 1. One can note that the LIGBT structure has a unique abrupt highly doped p++/n++ tunnel junction in the side of the collector. Using shallow trench isolation in the drift region can reduce the

potential crowding and peak electric field under the gate end and near the collector, thus the device reliability can be improved. Moreover, in switching applications there is no current convergence effect because of the n++ layer covering all over the collector region. The doping concentration of the p++ layer is equal to that of the n++ layer (of the order of 10^{20} cm^{-3}). The n++ layer has to be very thin, with its thickness being of the order of several to several tens of nanometres (set to be 50 nm in this Letter). The cell length L_{cell} in the x -direction is 24 μm . The drift region doping N_D is $2 \times 10^{15}\text{ cm}^{-3}$, and its length L_D is kept to 18 μm . The carrier lifetime $\tau = 0.1\text{ }\mu\text{s}$ is used at room temperature.

The operating principle of the tunnel-LIGBT is based on band-to-band tunnelling, which takes place in this device between the p++/n++ tunnel junction in the side of collector. It is worth noting that the static characteristics are the result of three current components: band-to-band tunnelling current, excess current and diffusion current. The energy band structure of the tunnel-LIGBT along the tunnel junction in the vertical y -direction is shown in Fig. 2 for different values of the applied collector voltage V_{CE} , depicting the band alignment. In the forward conducting mode, the collector is positively biased with a gate voltage ($V_{\text{GE}} > V_{\text{th}}$, where V_{th} is the threshold voltage), and accordingly the tunnel

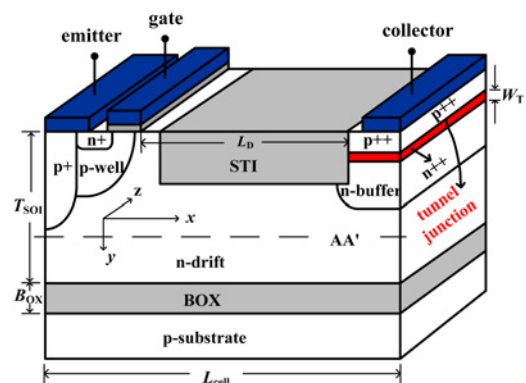


Figure 1 Schematic cross-section of the proposed tunnel-LIGBT with a band-to-band tunnel junction

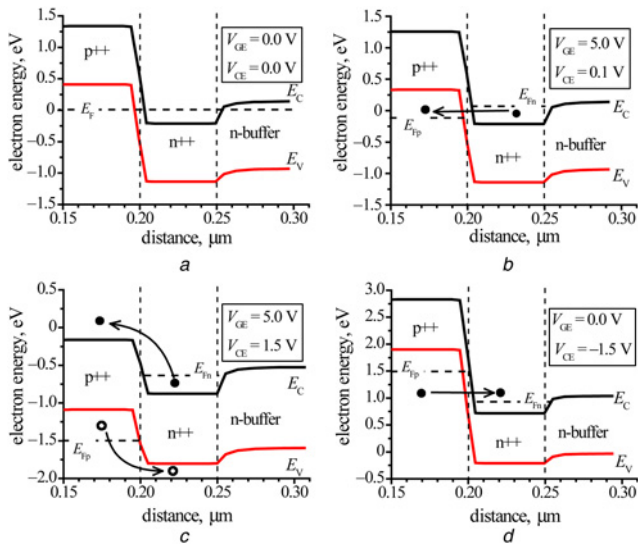


Figure 2 Simulated energy band diagrams of the tunnel junction in the vertical y -direction for the tunnel-LIGBT

- a Thermal equilibrium, zero bias
b Forward bias, the point of the tunnelling current peak
c Forward bias, with diffusion current and no tunnelling current
d Reverse bias, with the tunnelling current from E_V into E_C

junction is also forward biased. As the forward bias voltage increases, the electrons can tunnel from the conduction band to the valence band (shown in Fig. 2b from $n++$ side to $p++$ side). Then the tunnel current takes the lead in total current. The forward bias voltage further increases, the conduction band and the valence band are uncrossed and the tunnelling current drops to near 0 and with further increase of the voltage the normal diffusion current and excess current start to dominate (shown in Fig. 2c).

In the reverse conducting mode, the collector is negatively biased, and accordingly the tunnel junction is also reverse biased. When the gate voltage is greater than the threshold voltage ($V_{GE} > V_{th}$), the collector current increases monotonically. When $V_{GE} < V_{th}$, the operation of the tunnel-LIGBT is similar to that of a conventional diode. The electrons can tunnel from the valence band into the conduction band (shown in Fig. 2d). Thus, the built-in diode of the tunnel-LIGBT is equivalent to a p-n diode in series with a reverse tunnel junction.

Local tunnelling models (such as the Schenk model) adopted in their simulation work [16] assume either an average or maximum electric field which is constant throughout the tunnelling path. In fact, the tunnelling current depends on the band edge profile along the entire path between the points connected by tunnelling, which means the electric field at each point in the tunnelling path is dynamically changing. This makes tunnelling a non-local process but not a local process. To describe the non-local tunnelling process more accurately, we have used the non-local BTBT model in the Atlas device simulations (especially for the degenerately doped semiconductor device). The non-local BTBT current density across the tunnel junction with longitudinal energy E and transverse energy E_T is given by [17]

$$J_T = \frac{q}{\pi\hbar} \cdot \iint T_{WKB}(f_1 - f_2)\rho(E_T) dE dE_T \quad (1)$$

where $\rho(E_T)$ is the density of states corresponding to E_T . f_1 and f_2 are the Fermi-Dirac function using the quasi-Fermi level on the upside and the downside of the tunnel junction, respectively. T_{WKB} is the tunnelling probability, which is calculated using the WKB

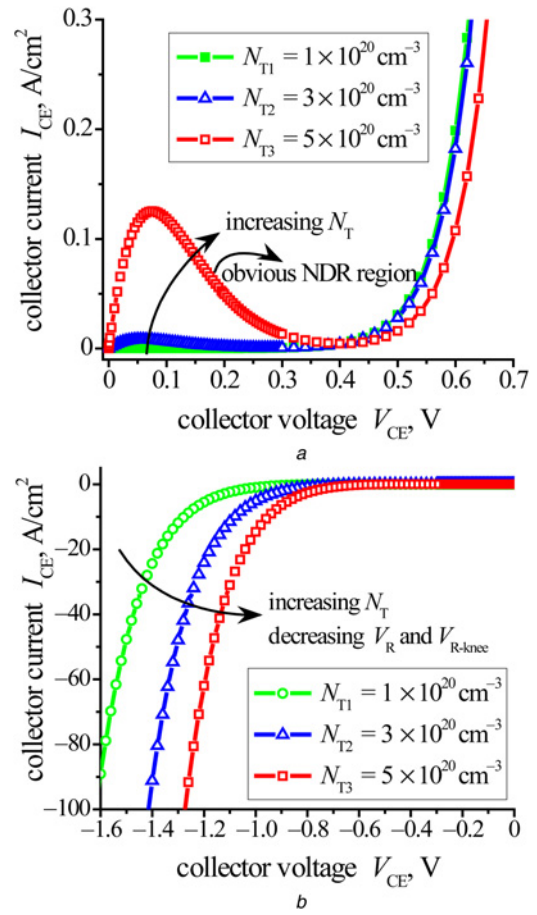


Figure 3 Static I - V characteristics of the tunnel-LIGBT for different doping concentrations of the $p++/n++$ layer

- a Forward conducting state ($V_{GE} = 5$ V)
b Reverse conducting state ($V_{GE} = 0$ V)

approximation as

$$T_{WKB} = \exp \left[-2 \int k_e k_h (k_e^2 + k_h^2)^{-1/2} dy \right] \quad (2)$$

where k_e and k_h are the evanescent wave vectors in the tunnelling direction for the electrons and the holes, respectively.

3. Results and discussion: The BTBT current of the proposed LIGBT is largely relevant to the doping concentration of the $n++$ layer near the collector. When below 100 nm, the width of the $n++$ layer does not affect the performance significantly [14]. Thus, the doping N_T of the $n++$ layer is an important parameter to be designed for proper optimisation. Fig. 3 shows the static forward and reverse I - V characteristics of the tunnel-LIGBT for different doping of the $n++$ layer. Fig. 3a illustrates that the maximum peak current I_P and the peak voltage V_P increase with an increasing N_T . When $N_T = 5 \times 10^{20} \text{ cm}^{-3}$, there has been a visible negative differential resistance (NDR) region ($I_P = 0.13 \text{ A/cm}^2$, $V_P = 0.085 \text{ V}$) and that is acceptable in its applications. However, the forward voltage drop at $N_T = 5 \times 10^{20} \text{ cm}^{-3}$ is noticeably increasing because the larger N_T limits the injection efficiency of the collector. From Fig. 3b, it can be observed that the tunnel-LIGBT with higher doping concentrations shows the lower reverse conduction voltage drop V_R at the same current density level. It is also worth noting that the reverse knee voltage V_{R-knee} decreases with increase of the doping N_T . This is because the lower N_T leads to a larger tunnelling barrier width. Thus, we can set N_T to be $3 \times 10^{20} \text{ cm}^{-3}$ ($V_{R-knee} = -1 \text{ V}$, $V_R = -1.4 \text{ V}$ at a

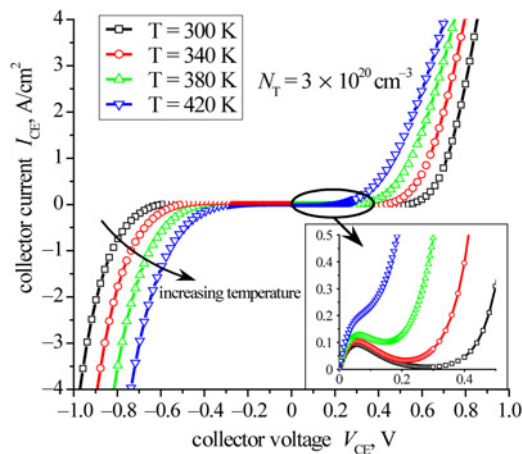


Figure 4 Collector current against collector voltages for increasing temperature from 300 to 420 K

reverse current density of 100 A/cm²) for trade-off consideration, and there is no obvious NDR region.

Fig. 4 shows the collector current against collector voltages for increasing temperatures from 300 to 420 K. As expected, the collector forward and reverse current increase as the temperatures increases. It is worth noting that the NDR region would gradually disappear with the increase of temperature (shown in the inset of Fig. 4). This behaviour can be explained by the narrowing of the bandgap with an increase in temperature; this is a joint effect of exponential increases of the band-to-band tunnelling current and the diffusion current.

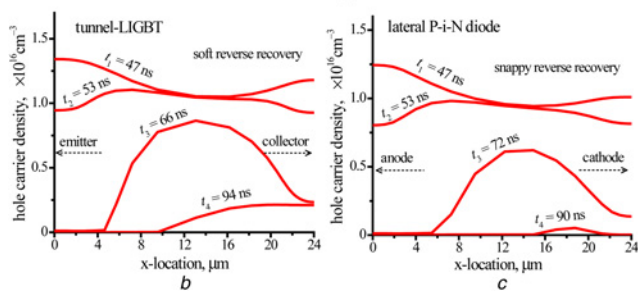
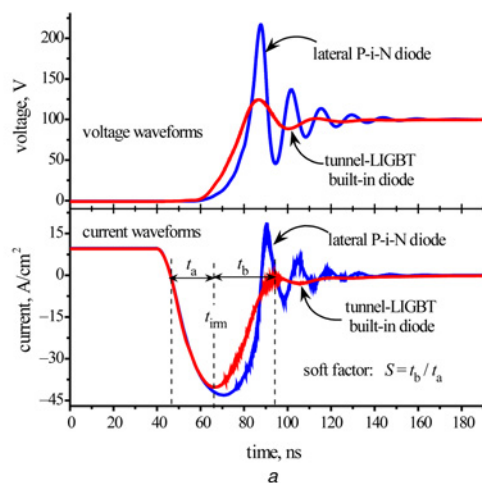


Figure 5 Comparison of the reverse recovery performances for the tunnel-LIGBT and the lateral P-i-N diode

a Reverse recovery waveforms (voltage and current waveforms)
b Carrier distributions (hole density) for the tunnel-LIGBT (along line AA' in Fig. 1)
c Carrier distributions (hole density) for the lateral P-i-N diode

For the conventional LIGBT, it is necessary to integrate an additional diode to match the LIGBT chip for obtaining soft recovery performance. Moreover, just the tunnel junction of the proposed LIGBT has good reverse conducting capability. This is the primary advantage of the tunnel-LIGBT. Thus, the tunnel junction can make the proposed LIGBT and the built-in diode to be an integrated structure without an additional diode. Reverse recovery waveforms of the tunnel-LIGBT during the reverse recovery process are shown in Fig. 5a. Figs. 5b and c show the carrier distributions along AA' in the drift region during the reverse recovery process for the tunnel-LIGBT and the lateral P-i-N diode. Although the reverse recovery time t_{rr} of the tunnel-LIGBT is slightly larger than that of the lateral P-i-N diode, the lateral P-i-N diode shows hard recovery characteristics and a clear current snap-off and a sharp voltage overshoot, whereas the tunnel-LIGBT exhibits a very soft current tail and a lower peak reverse recovery current. At the end of the reverse recovery process in the tunnel-LIGBT, the collector starts to emit holes into the n-drift region, so it can support the soft reverse recovery current and prevent a snap-off from occurring. From Fig. 5, we can see that the soft factor S of the tunnel-LIGBT built-in diode is 1.42, which is about two times better than that of the lateral P-i-N diode ($S=0.72$). So this progress in the built-in diode of the tunnel-LIGBT can lead to an advantage at the system level, which might well justify the necessary effort.

4. Conclusion: In summary, we have presented a novel LIGBT structure with a non-local band-to-band tunnelling junction at the collector region. The reverse-biased characteristic of the tunnelling junction is utilised to successfully achieve the reverse conducting and reverse recovery capability of the proposed LIGBT. The reverse recovery performances of the built-in diode can also be improved drastically and the soft factor of the proposed LIGBT became about two times better than that of lateral P-i-N diode. It is thus a promising device to be used in power ICs.

5. Acknowledgments: This work was supported by the National Science and Technology Major Project (Grant no. 2011ZX02706-003) and the National Natural Science Foundation of China (Grant no. 61076082).

6 References

- [1] Qian Q., Sun W., Liu S., Zhu J.: 'Novel hot-carrier degradation mechanisms in the lateral insulated-gate bipolar transistor on SOI substrate', *IEEE Trans. Electron Devices*, 2011, **58**, pp. 1158–1163
- [2] Fu Q., Zhang B., Luo X., Wang Z., Li Z.J.: 'Small-sized silicon-on-insulator lateral insulated gate bipolar transistor for larger forward bias safe operating area and lower turnoff energy', *Micro Nano Lett.*, 2013, **8**, pp. 386–389
- [3] Esteve V., Sanchis-Kilders E., Jordan J., *ET AL.*: 'Improving the efficiency of IGBT series-resonant inverters using pulse density modulation', *IEEE Trans. Ind. Electron.*, 2011, **58**, pp. 979–987
- [4] Udrea F.: 'SOI-based devices and technologies for high voltage ICs'. Proc. in IEEE BCTM, 2007, pp. 74–81
- [5] Letavic T., Petruzzello J., Claes J., Eggenkamp P., Janssen E., van der Wal A.: '650 V SOI LIGBT for switch-mode power supply application'. Proc. IEEE ISPSD, 2006, pp. 1–4
- [6] Green D.W., Vershinin K.V., Sweet M., Narayanan E.M.S.: 'Anode engineering for the insulated gate bipolar transistor – a comparative review', *IEEE Trans. Power Electron.*, 2007, **22**, pp. 1857–1866
- [7] Takahashi H., Yamamoto A., Anon S., Minato T.: '1200 V reverse conducting IGBT'. Proc. IEEE ISPSD, 2004, pp. 133–136
- [8] Simpson M.R.: 'Analysis of negative differential resistance in the I - V characteristics of shorted-anode LIGBT's', *IEEE Trans. Electron Devices*, 1991, **38**, pp. 1633–1640
- [9] Esaki L.: 'New phenomenon in narrow germanium p-n junctions', *Phys. Rev. B*, 1958, **109**, pp. 603–604

- [10] Ionescu A.M., Riel H.: 'Tunnel field-effect transistors as energy-efficient electronic switches', *Nature*, 2011, **479**, pp. 329–337
- [11] Seabaugh A.C., Zhang Q.: 'Low-voltage tunnel transistors for beyond CMOS logic', *Proc. IEEE*, 2010, **98**, pp. 2095–2110
- [12] Lattanzio L., Biswas A., Michielis L.D., Ionescu A.M.: 'A tunneling field-effect transistor exploiting internally combined band-to-band and barrier tunneling mechanisms', *Appl. Phys. Lett.*, 2011, **98**, pp. 123504.1–123504.3
- [13] Autran J.L., Munteanu D.: 'Tunneling component of the ballistic current in ultimate double-gate devices', *Electrochem. Solid-State Lett.*, 2003, **6**, pp. G95–G97
- [14] Hua Y., Haldar P.: 'A MOS gated power semiconductor switch using band-to-band tunneling and avalanche injection mechanism', *IEEE Trans. Electron Devices*, 2008, **55**, pp. 1524–1528
- [15] Goyal N., Saxena R.S.: 'A new LDMOSFET with tunneling junction for improved on-state performance', *IEEE Electron Device Lett.*, 2013, **34**, pp. 90–92
- [16] Jiang H., Wei J., Zhang B., Chen W., Qiao M., Li Z.: 'Band-to-band tunneling injection insulated-gate bipolar transistor with a soft reverse-recovery built-in diode', *IEEE Electron Device Lett.*, 2012, **33**, pp. 1684–1686
- [17] Atlas User's Manual: Device Simulation Software: Silvaco Int., 2010